Two-photon excited autofluorescence imaging of freshly isolated frog retinas

Rong-Wen Lu,[1] Yi-Chao Li,[1] Tong Ye,[2] Christianne Strang,[3] Kent Keyser,[3] Christine A. Curcio,[4] and Xin-Cheng Yao[1*]

[1]*Department of Biomedical Engineering, University of Alabama at Birmingham, Birmingham, AL 35294, USA*
[2]*Department of Neurobiology, University of Alabama at Birmingham, Birmingham, AL 35294*
[3]*Department of Vision Sciences, University of Alabama at Birmingham, Birmingham, AL 35294*
[4]*Department of Ophthalmology, University of Alabama at Birmingham, Birmingham, AL 35294*
**xcy@uab.edu*

Abstract: The purpose of this study was to investigate cellular sources of autofluorescence signals in freshly isolated frog (*Rana pipiens*) retinas. Equipped with an ultrafast laser, a laser scanning two-photon excitation fluorescence microscope was employed for sub-cellular resolution examination of both sliced and flat-mounted retinas. Two-photon imaging of retinal slices revealed autofluorescence signals over multiple functional layers, including the photoreceptor layer (PRL), outer nuclear layer (ONL), outer plexiform layer (OPL), inner nuclear layer (INL), inner plexiform layer (IPL), and ganglion cell layer (GCL). Using flat-mounted retinas, depth-resolved imaging of individual retinal layers further confirmed multiple sources of autofluorescence signals. Cellular structures were clearly observed at the PRL, ONL, INL, and GCL. At the PRL, the autofluorescence was dominantly recorded from the intracellular compartment of the photoreceptors; while mixed intracellular and extracellular autofluorescence signals were observed at the ONL, INL, and GCL. High resolution autofluorescence imaging clearly revealed mosaic organization of rod and cone photoreceptors; and sub-cellular bright autofluorescence spots, which might relate to connecting cilium, was observed in the cone photoreceptors only. Moreover, single-cone and double-cone outer segments could be directly differentiated.

© 2011 Optical Society of America

OCIS codes: (170.2655) Functional monitoring and imaging; (170.4580) Optical diagnostics for medicine; (170.3880) Medical and biological imaging; (330.5380) Physiology

References and links

1. G. R. Jackson, C. Owsley, and C. A. Curcio, "Photoreceptor degeneration and dysfunction in aging and age-related maculopathy," Ageing Res. Rev. **1**(3), 381–396 (2002).
2. R. E. Hogg and U. Chakravarthy, "Visual function and dysfunction in early and late age-related maculopathy," Prog. Retin. Eye Res. **25**(3), 249–276 (2006).
3. B. Meyer-Rüsenberg, M. Pavlidis, T. Stupp, and S. Thanos, "Pathological changes in human retinal ganglion cells associated with diabetic and hypertensive retinopathy," Graefes Arch. Clin. Exp. Ophthalmol. **245**(7), 1009–1018 (2007).
4. Y. Qin, G. Xu, and W. Wang, "Dendritic abnormalities in retinal ganglion cells of three-month diabetic rats," Curr. Eye Res. **31**(11), 967–974 (2006).
5. R. S. Harwerth and H. A. Quigley, "Visual field defects and retinal ganglion cell losses in patients with glaucoma," Arch. Ophthalmol. **124**(6), 853–859 (2006).
6. R. W. Nickells, "Ganglion cell death in glaucoma: from mice to men," Vet. Ophthalmol. **10**(s1 Suppl 1), 88–94 (2007).
7. B. Chance, "Pyridine nucleotide as an indicator of the oxygen requirements for energy-linked functions of mitochondria," Circ. Res. **38**(5 Suppl 1), I31–I38 (1976).
8. S. Bearelly, A. A. Khanifar, D. E. Lederer, J. J. Lee, J. H. Ghodasra, S. S. Stinnett, and S. W. Cousins, "Use of fundus autofluorescence images to predict geographic atrophy progression," Retina **31**(1), 81–86 (2011).
9. F. C. Delori, C. K. Dorey, G. Staurenghi, O. Arend, D. G. Goger, and J. J. Weiter, "*In vivo* fluorescence of the ocular fundus exhibits retinal pigment epithelium lipofuscin characteristics," Invest. Ophthalmol. Vis. Sci. **36**(3), 718–729 (1995).

#143592 - $15.00 USD Received 3 Mar 2011; revised 7 May 2011; accepted 7 May 2011; published 11 May 2011

10. O. La Schiazza and J. F. Bille, "High-speed two-photon excited autofluorescence imaging of *ex vivo* human retinal pigment epithelial cells toward age-related macular degeneration diagnostic," J. Biomed. Opt. **13**(6), 064008 (2008).
11. Y. Imanishi, K. H. Lodowski, and Y. Koutalos, "Two-photon microscopy: shedding light on the chemistry of vision," Biochemistry **46**(34), 9674–9684 (2007).
12. A. D. Marmorstein, L. Y. Marmorstein, H. Sakaguchi, and J. G. Hollyfield, "Spectral profiling of autofluorescence associated with lipofuscin, Bruch's Membrane, and sub-RPE deposits in normal and AMD eyes," Invest. Ophthalmol. Vis. Sci. **43**(7), 2435–2441 (2002).
13. D. Schweitzer, S. Schenke, M. Hammer, F. Schweitzer, S. Jentsch, E. Birckner, W. Becker, and A. Bergmann, "Towards metabolic mapping of the human retina," Microsc. Res. Tech. **70**(5), 410–419 (2007).
14. J. C. Hwang, D. Y. Kim, C. L. Chou, and S. H. Tsang, "Fundus autofluorescence, optical coherence tomography, and electroretinogram findings in choroidal sclerosis," Retina **30**(7), 1095–1103 (2010).
15. A. Bindewald-Wittich, M. Han, S. Schmitz-Valckenberg, S. R. Snyder, G. Giese, J. F. Bille, and F. G. Holz, "Two-photon-excited fluorescence imaging of human RPE cells with a femtosecond Ti:sapphire laser," Invest. Ophthalmol. Vis. Sci. **47**(10), 4553–4557 (2006).
16. Y. Hagiwara, K. Hattori, T. Aoki, H. Ohgushi, and H. Ito, "Autofluorescence assessment of extracellular matrices of a cartilage-like tissue construct using a fluorescent image analyser," J. Tissue Eng. Regen. Med. **5**(2), 163–168 (2011).
17. H. Hillman, T. Hussain, and P. Sartory, "Autofluorescence of isolated unfixed rabbit Deiters' neurons and surrounding neuroglial clamps," Experientia **29**(9), 1113–1115 (1973).
18. K. C. Reinert, R. L. Dunbar, W. C. Gao, G. Chen, and T. J. Ebner, "Flavoprotein autofluorescence imaging of neuronal activation in the cerebellar cortex *in vivo*," J. Neurophysiol. **92**(1), 199–211 (2004).
19. J. I. Morgan, J. J. Hunter, W. H. Merigan, and D. R. Williams, "The reduction of retinal autofluorescence caused by light exposure," Invest. Ophthalmol. Vis. Sci. **50**(12), 6015–6022 (2009).
20. J. I. W. Morgan, A. Dubra, R. Wolfe, W. H. Merigan, and D. R. Williams, "*In vivo* autofluorescence imaging of the human and macaque retinal pigment epithelial cell mosaic," Invest. Ophthalmol. Vis. Sci. **50**(3), 1350–1359 (2009).
21. K. Grieve and A. Roorda, "Intrinsic signals from human cone photoreceptors," Invest. Ophthalmol. Vis. Sci. **49**(2), 713–719 (2008).
22. F. Romero-Borja, K. Venkateswaran, A. Roorda, and T. Hebert, "Optical slicing of human retinal tissue *in vivo* with the adaptive optics scanning laser ophthalmoscope," Appl. Opt. **44**(19), 4032–4040 (2005).
23. C. H. Chen, E. Tsina, M. C. Cornwall, R. K. Crouch, S. Vijayaraghavan, and Y. Koutalos, "Reduction of all-trans retinal to all-trans retinol in the outer segments of frog and mouse rod photoreceptors," Biophys. J. **88**(3), 2278–2287 (2005).
24. Q. Q. Wu, C. H. Chen, and Y. Koutalos, "All-trans retinol in rod photoreceptor outer segments moves unrestrictedly by passive diffusion," Biophys. J. **91**(12), 4678–4689 (2006).
25. M. Han, A. Bindewald-Wittich, F. G. Holz, G. Giese, M. H. Niemz, S. Snyder, H. Sun, J. Y. Yu, M. Agopov, O. La Schiazza, and J. F. Bille, "Two-photon excited autofluorescence imaging of human retinal pigment epithelial cells," J. Biomed. Opt. **11**(1), 010501 (2006).
26. M. Han, G. Giese, S. Schmitz-Valckenberg, A. Bindewald-Wittich, F. G. Holz, J. Y. Yu, J. F. Bille, and M. H. Niemz, "Age-related structural abnormalities in the human retina-choroid complex revealed by two-photon excited autofluorescence imaging," J. Biomed. Opt. **12**(2), 024012 (2007).
27. J. M. Bueno, E. J. Gualda, and P. Artal, "Adaptive optics multiphoton microscopy to study *ex vivo* ocular tissues," J. Biomed. Opt. **15**(6), 066004 (2010).
28. E. J. Gualda, J. M. Bueno, and P. Artal, "Wavefront optimized nonlinear microscopy of *ex vivo* human retinas," J. Biomed. Opt. **15**(2), 026007 (2010).
29. L. L. Zhao, J. L. Qu, D. N. Chen, and H. B. Niu, "Layered-resolved autofluorescence imaging of photoreceptors using two-photon excitation," J. Biomed. Sci. Eng. **02**(05), 363–365 (2009).
30. P. Yan, A. Xie, M. Wei, and L. M. Loew, "Amino(oligo)thiophene-based environmentally sensitive biomembrane chromophores," J. Org. Chem. **73**(17), 6587–6594 (2008).
31. Y. C. Li, C. Strang, F. R. Amthor, L. Liu, Y. G. Li, Q. X. Zhang, K. Keyser, and X. C. Yao, "Parallel optical monitoring of visual signal propagation from the photoreceptors to the inner retina layers," Opt. Lett. **35**(11), 1810–1812 (2010).
32. Y. B. Zhao and X. C. Yao, "Intrinsic optical imaging of stimulus-modulated physiological responses in amphibian retina," Opt. Lett. **33**(4), 342–344 (2008).
33. Q. X. Zhang, J. Y. Wang, L. Liu, and X. C. Yao, "Microlens array recording of localized retinal responses," Opt. Lett. **35**(22), 3838–3840 (2010).
34. X. C. Yao and Y. B. Zhao, "Optical dissection of stimulus-evoked retinal activation," Opt. Express **16**(17), 12446–12459 (2008).
35. Y. G. Li, Q. X. Zhang, L. Liu, F. R. Amthor, and X. C. Yao, "High spatiotemporal resolution imaging of fast intrinsic optical signals activated by retinal flicker stimulation," Opt. Express **18**(7), 7210–7218 (2010).
36. Y. G. Li, L. Liu, F. Amthor, and X. C. Yao, "High-speed line-scan confocal imaging of stimulus-evoked intrinsic optical signals in the retina," Opt. Lett. **35**(3), 426–428 (2010).
37. X. C. Yao, A. Yamauchi, B. Perry, and J. S. George, "Rapid optical coherence tomography and recording functional scattering changes from activated frog retina," Appl. Opt. **44**(11), 2019–2023 (2005).
38. X. C. Yao and J. S. George, "Near-infrared imaging of fast intrinsic optical responses in visible light-activated amphibian retina," J. Biomed. Opt. **11**(6), 064030 (2006).

#143592 - $15.00 USD Received 3 Mar 2011; revised 7 May 2011; accepted 7 May 2011; published 11 May 2011
(C) 2011 OSA

39. X. C. Yao and J. S. George, "Dynamic neuroimaging of retinal light responses using fast intrinsic optical signals," Neuroimage **33**(3), 898–906 (2006).
40. P. A. Sieving, K. Murayama, and F. Naarendorp, "Push-pull model of the primate photopic electroretinogram: a role for hyperpolarizing neurons in shaping the b-wave," Vis. Neurosci. **11**(03), 519–532 (1994).
41. S. E. Nilsson, "An electron microscopic classification of the retinal receptors of the leopard frog (*Rana pipiens*)," J. Ultrastruct. Res. **10**(5-6), 390–416 (1964).
42. P. A. Liebman and G. Entine, "Visual pigments of frog and tadpole (*Rana pipiens*)," Vision Res. **8**(7), 761–775, IN1–IN7 (1968).
43. V. Ramamurthy and M. Cayouette, "Development and disease of the photoreceptor cilium," Clin. Genet. **76**(2), 137–145 (2009).
44. T. Wakabayashi, M. Sawa, F. Gomi, and M. Tsujikawa, "Correlation of fundus autofluorescence with photoreceptor morphology and functional changes in eyes with retinitis pigmentosa," Acta Ophthalmol. (Copenh.) **88**(5), e177–e183 (2010).

1. Introduction

Functional evaluation of the retina is important for early detection and treatment evaluation of eye diseases, such as age-related macular degeneration (AMD) [1,2], diabetic retinopathy (DR) [3,4], and glaucoma [5,6]. Previous investigations have demonstrated that autofluorescence alterations could be used to detect metabolic parameters such as partial pressure of oxygen [7] in biological tissues, and could also act as unique biomarker for selective evaluation of individual cell types such as retinal pigment epithelium (RPE) [8–12]. Without complexities of sample preparation and potential toxicity of exogenous biomarkers, autofluorescence imaging of endogenous fluorophores promises a noninvasive method for functional measurement of the retina [13]. Fundus imaging has revealed autofluorescence from choroidal vessels and the retinal pigment epithelium (RPE) [14]. In principle, fundus autofluorescence imaging may provide high resolution identification of localized retinal dysfunction and thus allow improved disease detection and treatment evaluation. However, multiple types of retinal cells may contribute to fundus autofluorescence. Previous investigations of the retina [11,15] and other systems [16–18] have revealed that abundant endogenous fluorophores exist in both intracellular and extracellular compartments of biological tissues. Therefore, better understanding of cellular sources of fundus autofluorescence is essential to pursue advanced applications of this imaging technology.

Because of ocular aberrations and complex retinal structure, *in vivo* evaluation of the autofluorescence correlated with individual retinal cell types is challenging. In coordination with adaptive optics to compensate for ocular aberrations, *in vivo* autofluorescence imaging with cellular resolution in transverse direction has recently been demonstrated in macaque and human eyes [19,20]. However, axial resolution of adaptive optics imaging is limited, typically larger than the thickness of individual functional layers of the retina [21,22]. Therefore, *in vivo* dissection of the autofluorescence from individual retinal layers is still difficult.

Without the complication of ocular optics, isolated retinas can provide a simple *ex vivo* preparation for quantitative analysis of the contribution of individual retinal layers/cells, including the photoreceptor and inner retinal neurons, to the fundus autofluorescence. Fluorescence microscopy has been used to disclose robust autofluorescence in both outer and inner segments [23,24]. In principle, two-photon imaging can provide sub-cellular resolution in both transverse and axial directions to characterize autofluorescence in intact retinas. Recently, two-photon autofluorescence imaging of both fixed [11,15,25,26] and unfixed [27–29] *ex vivo* retinal preparations has been demonstrated. However, quantitative two-photon autofluorescence examination of the photoreceptor and inner retinal neurons has not been examined in freshly isolated, i.e., living, retinas. Early investigations suggested that excitation efficiencies and emitted spectra of the fluorophores can be very sensitive to various environmental factors such as partial pressure of oxygen, solvent polarity or viscosity, etc. [7,30]. Therefore, physiological solutions may provide for more accurate measurement of autofluorescence associated with live tissue.

The purpose of this study is to quantify two-photon excited autofluorescence signals from photoreceptors and inner neurons in freshly isolated retinas. In oxygenated Ringer's solution, freshly isolated retinas are viable and excitable, at least for a few hours. We have recently

#143592 - $15.00 USD Received 3 Mar 2011; revised 7 May 2011; accepted 7 May 2011; published 11 May 2011
(C) 2011 OSA

using freshly isolated retinas, including both sliced [31] and flat-mounted [32–39] retinas, to investigate stimulus-evoked retinal neural activities. In this study, the same retinal preparation, i.e., isolated but living retinas, to characterize cellular sources of retinal autofluorescence. In the freshly isolated retinas, robust autofluorescence signals were consistently observed across whole retinal depth, i.e., the photoreceptor layer (PRL), outer nuclear layer (ONL), outer plexiform layer (OPL), inner nuclear layer (INL), inner plexiform layer (IPL), and ganglion cell layer (GCL). Characteristic autofluorescence patterns were imaged over different retinal layers, and autofluorescence signals of individual retinal layers were quantitatively compared.

2. Method

2.1. Retinal preparation

Isolated leopard (*Rana pipiens*) frog retinas were used for the experiments. Isolated retinas provide a simple preparation to investigate cellular sources of autofluorescence in the retina without the complications associated with the presence of other ocular tissues and eye movements. Both sliced and flat-mounted retinas were used for this study. A retinal slice opens a cross-section of the retina, and thus allows simultaneous monitoring of autofluorescence signal from the photoreceptor outer segments to inner retina; while a flat-mounted retina allows depth-resolved imaging of individual retinal layers. The experimental procedures were approved by the Institutional Animal Care and Use Committee of University of Alabama at Birmingham. Details of the preparation of flat-mounted retinas [34] and retinal slices [31] have been previously reported. Briefly, retinal dissection was conducted in a dark room with dim red illumination. The frog was sacrificed by rapid decapitation and double pithing before the eyes were enucleated. The eyeball was hemisected below the equator with fine scissors to remove the lens and anterior structures before separating the retina from the retinal pigment epithelium. The isolated retina was directly used for flat-mounted imaging, or cut into ~200 μm slices for cross section imaging of the retina. During the recording, the retina was immersed in oxygenated Ringer's solution containing (in mM) [40]: 110 NaCl, 2.5 KCl, 1.6 $MgCl_2$, 1.0 $CaCl_2$, 22 $NaHCO_3$, and 10 D-glucose.

2.2. Experimental setup

Figure 1 shows a schematic diagram of the experimental setup. Equipped with an ultrafast mode-locked Ti:sapphire laser (Chameleon, Coherent Inc.), a laser scanning multi-photon microscope (Prairie Technologies) was used for two-photon exited autofluorescence imaging of freshly isolated retinas. During the recording, 720 nm laser pulses were selected for autofluorescence excitation of both flat-mounted retinas and retinal slices. Similar laser wavelength has been used for two-photon autofluorescence investigation of ocular tissues [11]. The width of each laser pulse was <140 fs, and the repetition rate was 90 MHz. The averaged laser power was adjusted between 2~10 mW which was measured at the specimen position and did not result in obvious damage of the retinal tissues. A high sensitivity photomultiplier tubes (PMT, H7422P, Hamamatsu Photonics) was employed for autofluorescence recording. A typical imaging frame (512 x 512 pixels) period used in the experiments was ~6.8 s, which corresponded to a 25.2 μs pixel dwell time (i.e. laser exposure time of each pixel).

3. Results

3.1. Autofluorescence imaging of retinal slices

The first step of this study was to verify multiple sources of autofluorescence signals in the retina. We started the experiments using freshly isolated frog retinal slices. Figure 2A represents conventional transmission image; while Fig. 2B represents two-photon exited autofluorescence image (Fig. 2B) of retinal slices. Figure 2C shows averaged autofluorescence signal at each depth of the retina shown in Fig. 2B. High resolution two-

#143592 - $15.00 USD Received 3 Mar 2011; revised 7 May 2011; accepted 7 May 2011; published 11 May 2011
(C) 2011 OSA

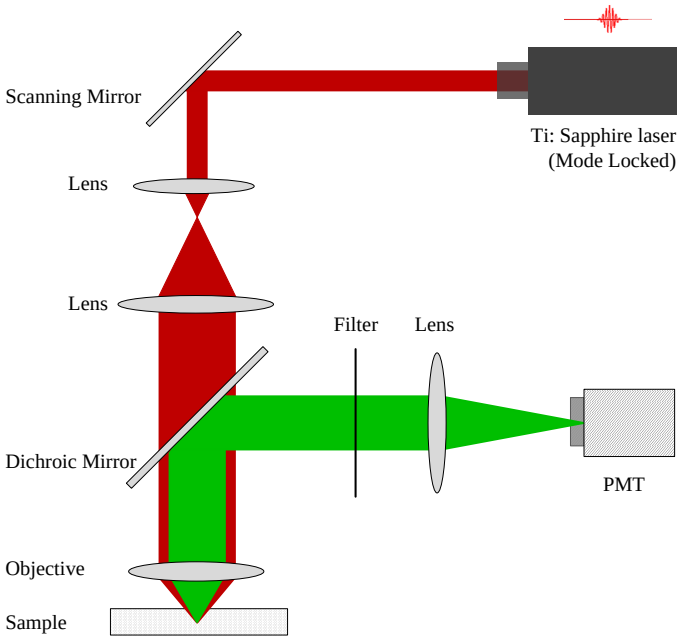

Fig. 1. Schematic diagram of the experimental setup for two-photon imaging of the frog retina. A mode-locked Ti:sapphire laser (Chameleon, Coherent Inc.) was used to provide excitation light (720 nm). At the dichroic mirror, the long-wavelength 720 nm excitation light (red rays) was passed through and the short-wavelength emission light (green rays) was reflected. A band-pass (450-550 nm) filter was placed in front of the photomultiplier tube (PMT).

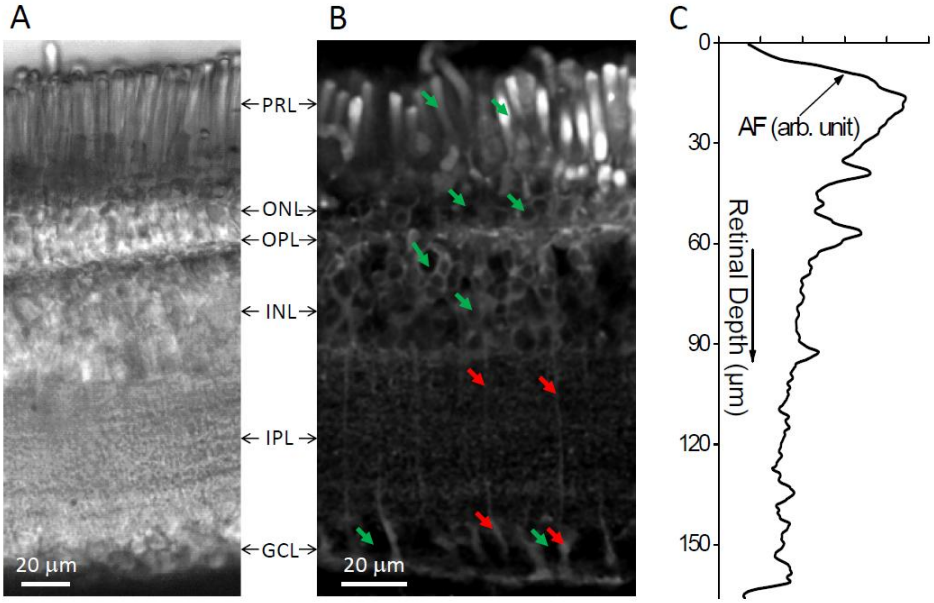

Fig. 2. (A) Transmission image of a frog retinal slice. During the recording, the retinal slice was continuously illuminated by an infrared (800-1000 nm) light. The PRL, ONL, OPL, INL, IPL, GCL could be directly differentiated. (B) Representative two-photon fluorescence image of frog retinal slices. The excitation light was set at 720 nm, and the average power is ~5 mW. In this image, single cellular structures (green arrowheads) were clearly observed in the PRL, ONL, INL, and GCL. Individual Müller glial cells (red arrowheads) were observed. (C) Averaged autofluorescence (AF) signal at each depth of the retinal slice shown in Fig. 2B.

#143592 - $15.00 USD Received 3 Mar 2011; revised 7 May 2011; accepted 7 May 2011; published 11 May 2011
(C) 2011 OSA

photon imaging disclosed robust autofluorescence from multiple retinal layers, including PRL, ONL, OPL, INL, IPL and GCL, with sub-cellular spatial resolution. Retinal slice experiments indicated that the 720 nm pulse laser can provide autofluorescence excitation of both photoreceptors and inner retinal cells. In comparison with the conventional transmission imaging (Fig. 2A), the two-photon autofluorescence measurement (Fig. 2B) showed significantly improved image contrast, allowing direct observation of single cells (green arrowheads in Fig. 2B) at individual functional layers, and also fiber like Müller glial cells that initiated from the GCL and penetrated into inner retinal layers (red arrowheads in Fig. 2B). Although autofluorescence signals were consistently observed throughout the retina, the signal efficiency of the outer retina, e.g., PRL, was significantly higher than that of inner retinal layers (Fig. 2C).

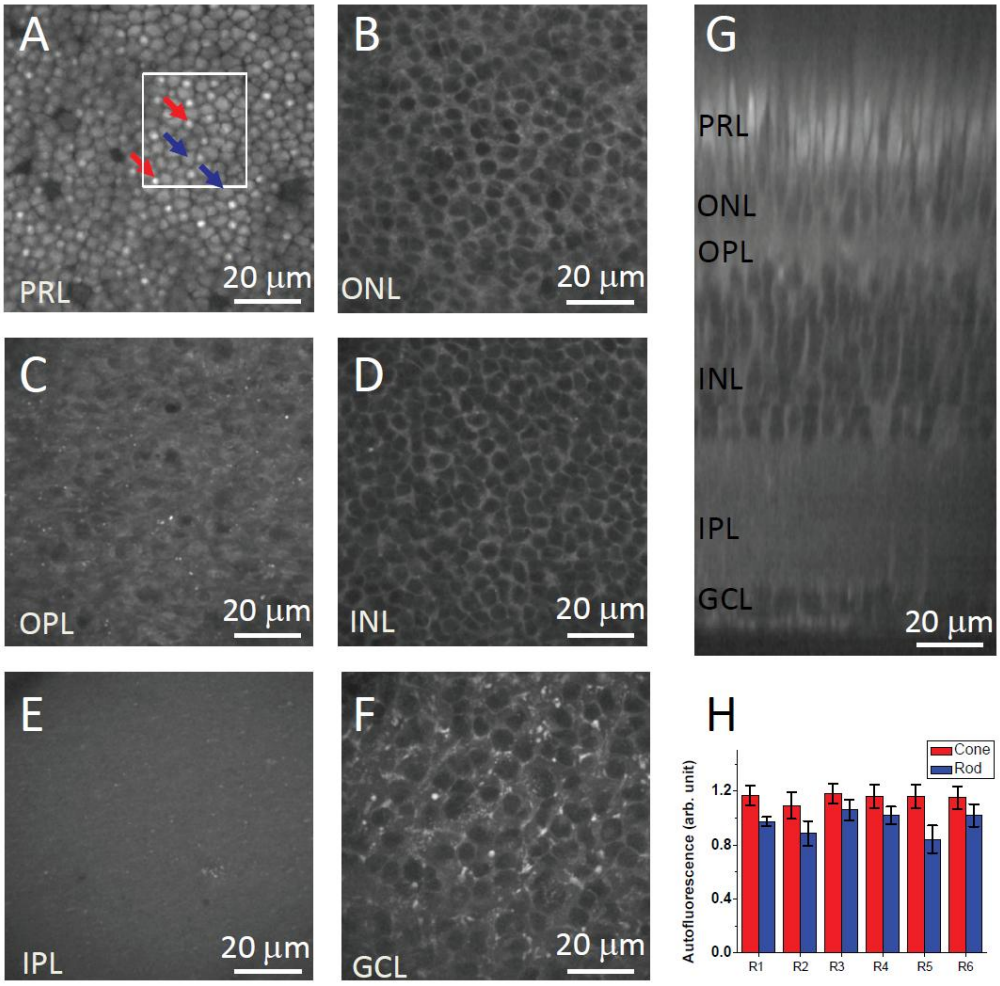

Fig. 3. Two-photon excited autofluorescence imaging of the flat-mounted retina. The 720 nm excitation light was delivered from the GCL side, i.e., the GCL side faced to the objective in Fig. 1. Two-photon images of the PRL (A), ONL (B), OPL (C), INL (D), IPL (E), and GCL (F), were collected with identical excitation power of ~10 mW. The white square in A marks the region of interest shown in greater detail in Fig. 4. (G) Depth-resolved scan, i.e., a cross-section, of a line area of the flat-mounted retina. (H) Comparison of rod and cone autofluorescence recorded from 6 retinal preparations R1-6. For each retina, 10 rods and 10 cones were randomly selected for average calculations of the rod and cone autofluorescence. The line bars indicate standard deviation.

#143592 - $15.00 USD Received 3 Mar 2011; revised 7 May 2011; accepted 7 May 2011; published 11 May 2011
(C) 2011 OSA

3.2. Autofluorescence imaging of flat-mounted retinas

The second phase of this study was to test the feasibility of depth-resolved imaging of two-photon excited autofluorescence in flat-mounted retinas, i.e., isolated but living retinas. Figures 3A–F represents two-photon images of the PRL, ONL, OPL, INL, IPL, and GCL, respectively. Figure 3G shows a cross-section scan, from the GCL to the PRL, of the flat-mounted retina. As shown in Fig. 3A, PRL autofluorescence was dominantly localized at intracellular compartment of individual photoreceptors; while ONL, INL and GCL autofluorescence images were dominated by extracellular signals, although mixed intracellular and extracellular patterns were observed. Different brightness of individual cells, which might reflect variable cell types, was observed. Bright spots were observed in the OPL and IPL (Figs. 3C and 3E). Mosaic pattern of rod and cone photoreceptors was clearly observed in Fig. 3A. The rod (blue arrowheads in Fig. 3A) and cone (red arrowheads in Fig. 3A) photoreceptors could be separated simply based on their cellular sizes. In general, the outer segment diameter of frog rods (~5-8 μm) is larger than that of the cones (~1-3 μm) [41,42]. Moreover, single and double cones could be further separated (green arrowheads in Fig. 4B). In overall, the cones show brighter autofluorescence than that of the rods (Fig. 3H).

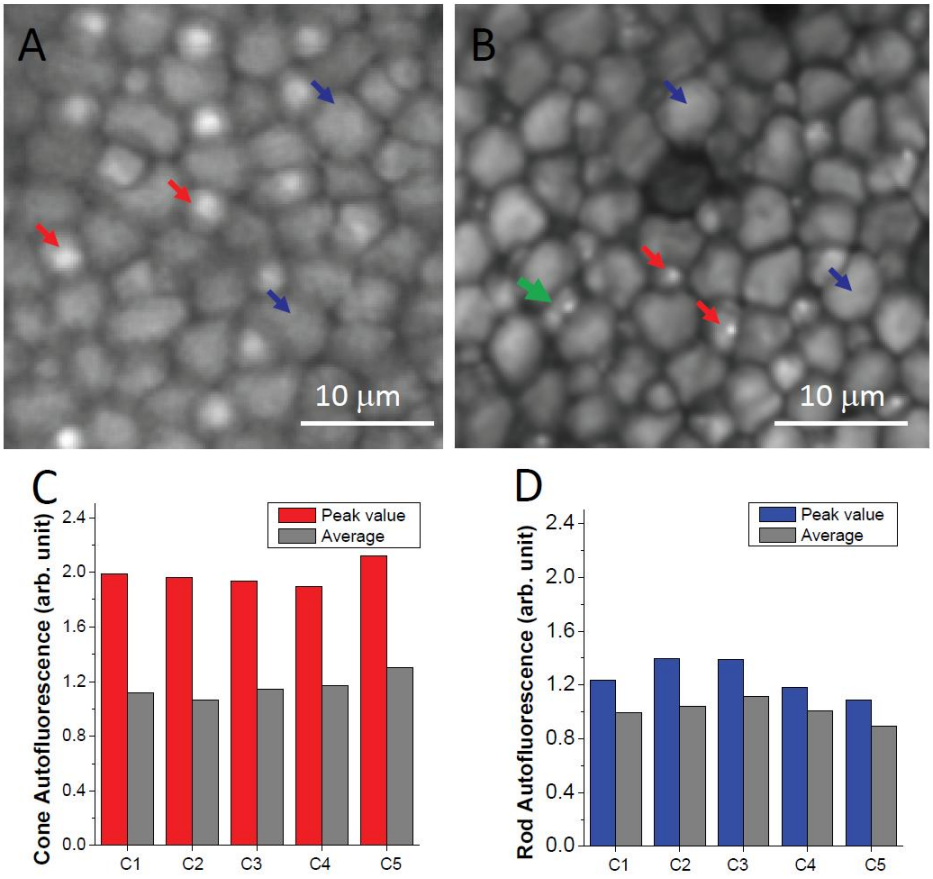

Fig. 4. (A) Enlarged PRL illustration of a sub-image marked by the white square in Fig. 3A. This image revealed that the rod (blue arrowheads) autofluorescence was relatively homogenous at the cellular level; while a bright spot with sub-cellular structure was frequently observed in the cones (red arrowheads). (B) Another example of autofluorescence image of the rod and cone mosaics. Bright autofluorescence spots were consistently observed in the cones (red arrowheads) and double cones (green arrowhead). (C) and (D) show peak and average values of 5 representative cones and 5 rods, respectively.

#143592 - $15.00 USD Received 3 Mar 2011; revised 7 May 2011; accepted 7 May 2011; published 11 May 2011
(C) 2011 OSA

Figure 4A shows enlarged PRL illustration of a sub-image marked by the white square in Fig. 3A. From Fig. 4A, we observed that the rod (blue arrowheads) autofluorescence was relatively homogenous at the cellular level; while distinct bright spots were frequently observed in the cones (red arrowheads). In order to demonstrate the repeatability of the experiment, Fig. 4B shows another example of autofluorescence image of the rod and cone mosaics. The peak value, i.e., the pixel value with highest brightness, of individual cones (Fig. 4C) was significantly (~1.7 times) larger than the average cone value; while the peak value of individual rods (Fig. 4D) was only slightly (~1.2 times) larger than the average rod value.

In order to further characterize the rod and cone autofluorescence, Fig. 5 shows depth-resolved image sequence of the PRL with a depth interval of 2 μm. During the recording, the transverse scanning step, i.e., pixel resolution was improved to 0.3 μm (compared to the 0.5 μm pixel size used for the experiments shown in Fig. 3 and Fig. 4). In order to minimize

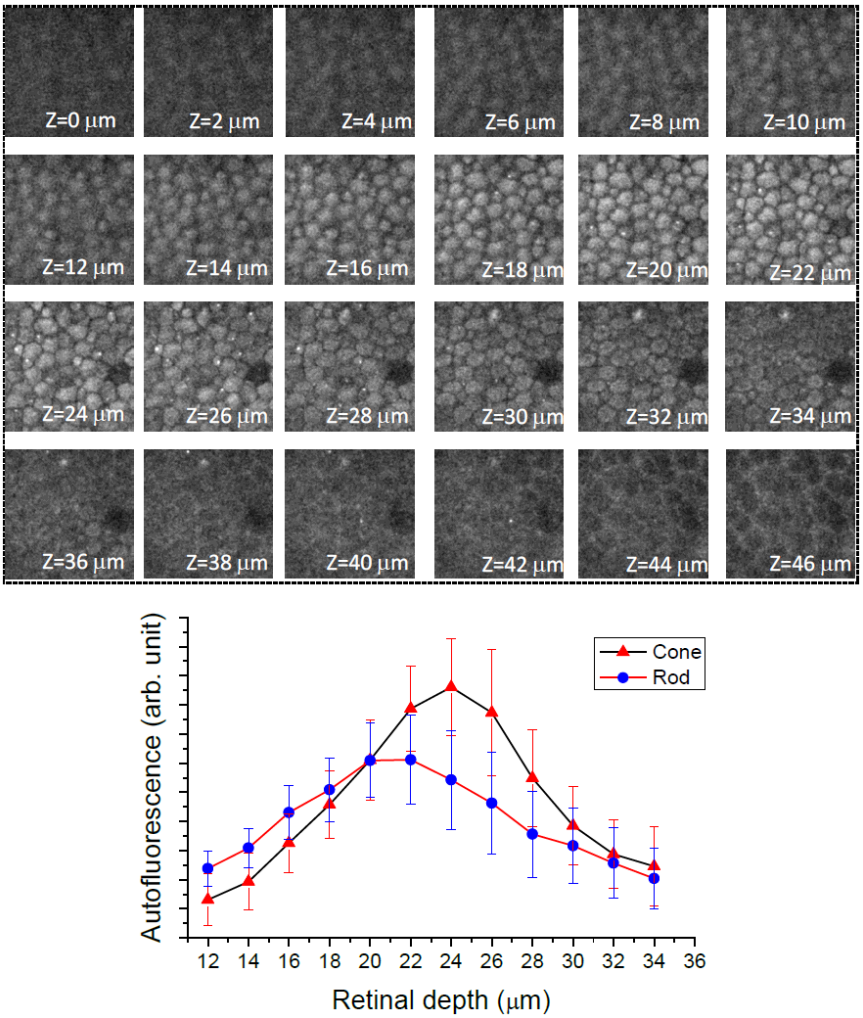

Fig. 5. Top panel shows depth-resolved imaging of the PRL autofluorescence. The images were collected with 2 μm depth interval and 0.3 μm pixel size. The excitation power was ~5 mW. A bright autofluorescence spot was frequently observed in the cone. Primary bright spots were localized at z = 16-30 μm relative to the PRL side retinal surface. Bottom panel is quantitative comparison of autofluorescence between rods and cones at z = 12-34 μm. At each depth, 6 rods and 6 cones were used for averaging. The line bars indicate standard deviation.

#143592 - $15.00 USD Received 3 Mar 2011; revised 7 May 2011; accepted 7 May 2011; published 11 May 2011
(C) 2011 OSA

signal cross-talk of adjacent rods and cones, the excitation power was lowered to ~5 mW (compared to the 10 mW used for the experiments shown in Fig. 3). High resolution two-photon imaging consistently revealed bright autofluorescence spots in the cones. Depth-resolved recording indicated that the bright spots were localized primarily at z = 16-30 μm, relative to the PRL side retinal surface.

3.3. Comparison of autofluorescence signals in retinal slices and flat-mounted retinas

In retinal slices, the autofluorescence sensitivity of the PRL was significantly higher than that of inner retinal layers (Figs. 2B and 2C). However, in flat-mounted retinas, relative fluorescence sensitivity, i.e., signal contrast to other retinal layers, of the PRL was compromised (Figs. 3A–H)). Figure 6 shows autofluorescence averages of the PRL, ONL, OPL, INL, IPL and GCL in retinal slices and flat-mounted retinas.

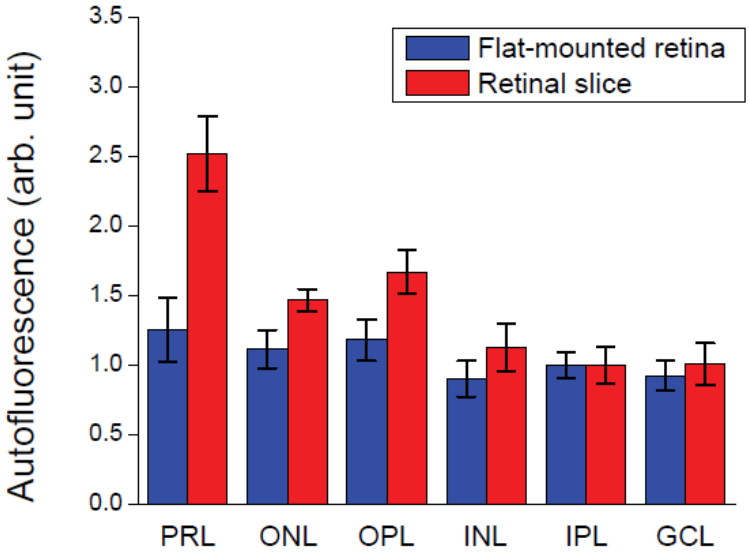

Fig. 6. Averaged autofluorescence of the PRL, ONL, OPL, INL, IPL and GCL. 6 retinal slices and 6 flat-mounted retinas were used for the average. Red and blue bars show the signals recorded from retinal slices and flat-mounted retinas, respectively. The line bars indicate standard deviation.

4. Discussion

In summary, two-photon excited autofluorescence imaging of freshly isolated frog retinas was conducted. Freshly isolated retinas could be maintained in a physiological environment that can minimize the differences from *in situ* metabolic status of living retinas. High resolution examination of the freshly isolated retinas verified multiple cellular sources, including the PRL, ONL, OPL, INL, IPL, and GCL of retinal autofluorescence. Both retinal slices and flat-mounted retinas were used for this study. Two-photon image of the retinal slice revealed that signal efficiency of the PRL was significantly higher than that of inner retinal layers, although autofluorescence signals were consistently observed over the whole thickness of the retina (Fig. 2C). In contrast, autofluorescence sensitivity of the PRL was compromised in flat-mounted retinas (Figs. 3A–H). This might result from reduced light efficiency due to light scattering, absorption, and aberration, in the flat-mounted retinal preparation.

At the PRL, autofluorescence was dominantly confined to the intracellular compartment. High-resolution imaging revealed the mosaic organization of rod and cone photoreceptors, and single and double cones could be identified (Fig. 3 and Fig. 4). Autofluorescence distribution in the rod outer segment was relatively homogenous; while sub-cellular bright spots with light intensity well above average level were revealed in the cone outer segment

#143592 - $15.00 USD Received 3 Mar 2011; revised 7 May 2011; accepted 7 May 2011; published 11 May 2011
(C) 2011 OSA

(Figs. 3 and 4). Early investigations suggested that autofluorescence signals of outer and inner photoreceptor segments were related to all-trans retinol and nicotinamide adenine dinucleotide phosphate (NADPH), respectively [11,23,26]. However, the observed bright autofluorescence spots in cones might not, at least not completely, result from the all-trans retinol. These bright spots were frequently observed at the periphery of the cones (Fig. 4). We speculate that the bright autofluorescence spots might be related to the connecting cilium (CC), which links the inner segments to the outer segments. It is well established that the CC constitutes a sort of highway for proteins, such as rhodopsin, travelling to and from the outer segment [43]. These proteins might contribute to the observed bright autofluorescence spots by producing autofluorescence signals directly. Alternatively, the CC might act as a light waveguide to affect the excitation and collection efficiency of all-trans retinol in sub-cellular locations, relative to the CC axis, in the cone outer segments. Early investigations indicated that the length of the cone outer segment is 7-13 μm [41], which is consistent with the observed depth range (~14 μm, i.e., z = 16-30 μm in Fig. 5) of the bright autofluorescence spots.

In other retinal layers, both intracellular and extracellular autofluorescence signals were observed. Cellular structures were clearly observed at the ONL, INL, and GCL, while bright autofluorescence spots, which might relate to individual nerve terminals, were observed in the OPL and IPL. According to previous investigations with retina and other biological tissues, the observed autofluorescence might result from reduced nicotinamide adenine dinucleotide (NADH) and reduced nicotinamide adenine dinucleotide phosphate (NADPH), collectively referred to as NAD(P)H, and the oxidized forms of flavoproteins [11]. Most of the NAD(P)H fluorescence originates from the mitochondria and can serve as the basis for redox fluorometry. Therefore, pyridine nucleotides and flavins not only can provide morphological contrast, but may also act as valuable biomarkers for functional imaging of metabolic activity of living tissues [11].

In conclusion, two-photon imaging of freshly isolated retinas revealed multiple, intracellular and extracellular, sources of endogenous fluorophores that were simultaneously excited by the constant-wavelength (720 nm) light from a pulsed laser. Because autofluorescence signals originated from both outer and inner retinal layers, signal specificity of fundus autofluorescence imaging is limited and cross-contamination among different cell types is not negligible. Further investigations are necessary to understand biophysical and biochemical mechanisms of retinal autofluorescence better. We are currently pursuing further experiments with mammalian retinas that have a closer similarity with human retinas to verify the autofluorescence inhomogeneity observed in the frog photoreceptors, and to characterize the autofluorescence mechanisms. In coordination with variable controls of excitation wavelength and spectral measurement, advanced investigations of retinal autofluorescence in the retina of animal models may provide insight in the development of a new imaging methodology for selective evaluation of the rod, cone, and inner retinal neurons, which may lead to better study and improved diagnosis of AMD [1,2], diabetic retinopathy (DR) [3,4], and glaucoma [5,6], retinitis pigmentosa (RP) [44], and other eye diseases that can produce functional damages of retinal cells.

Acknowledgments

This research is supported by the Dana Foundation (Brain and Immuno-Imaging Grant program), the Eyesight Foundation of Alabama, the National Institutes of Health (NIH) (5R21RR025788-02 and 1R21EB012264-01A1), and the National Science Foundation (CBET-1055889). The two-photon fluorescence images were acquired in the Neuroimaging Core, which was supported by NIH Neuroscience Blueprint Core Grant NS57098 to the University of Alabama at Birmingham.

#143592 - $15.00 USD Received 3 Mar 2011; revised 7 May 2011; accepted 7 May 2011; published 11 May 2011
(C) 2011 OSA